

## Operational Performance and Weld Bead Characteristics of Experimental Tubular-Wires for Underwater Welding

Orlando M. Castellanos-Gonzalez<sup>1</sup>, Eduardo J. Sanchez Lobo<sup>1</sup>, Dariusz Fydrych<sup>2</sup>,  
Bruno Silva Cota<sup>3</sup>, José Gedael Fagundes Júnior<sup>4</sup>, Andrés Mauricio Moreno-Urbe<sup>1\*</sup>

<sup>1</sup> Federal University of Minas Gerais- UFMG, Graduate Program in Mechanical Engineering, Belo Horizonte, MG, Brazil

<sup>2</sup> Institute of Manufacturing and Materials Technology, Faculty of Mechanical Engineering and Ship Technology, Gdańsk University of Technology, Gabriela Narutowicza 11/12, 80-233 Gdańsk, Poland

<sup>3</sup> Universidade Federal de Itajubá - UNIFEI, Instituto de Engenharias Integradas, Itabira, MG, Brazil

<sup>4</sup> São Paulo State University, Department of Mechanical Engineering, Ilha Solteira, SP, Brazil

\* Corresponding author's e-mail: andresmauriciomu@ufmg.br

### ABSTRACT

Aiming to evaluate new formulations and their operational behavior underwater, two experimental tubular wires with different chemical compositions in their internal flux were initially manufactured, employing a pilot machine and a unique manufacturing process. Weld beads were deposited on a plate placed in a flat position inside a tank using a mechanized system and the IMC 300 welding power source. The work was done at a depth of 0.3 meters of water, and both reverse and direct polarities were used. Arc voltage at 28 V, wire feed speed at 4.5 m/min and welding speed at 250 mm/min were maintained in all experiments. As a result, the weld bead morphology and the electrical variables related to arc voltage and welding current were analyzed. It was concluded that the metal transfer showed a predominance of short circuits and a decrease in the average value of the Short Circuit Index by 67% when using the positive polarity configuration compared to the negative polarity. Moreover, the average penetration value was 38 % higher for the oxidizing-based tubular wire than for the rutile-based tubular wire, which has a possible relationship with the more significant presence of oxygen in the flux. In addition, the results present an analysis of the performance of the process and the characterization of the weld beads obtained to guide possible modifications in the parameters.

**Keywords:** underwater wet welding, flux-cored arc welding, polarity, PTFE, electric arc welding.

### INTRODUCTION

The maintenance of structures used for oil and gas exploration, production, and transportation poses a challenge for offshore industry companies [1]. Consequently, the underwater welding technique facilitates the repair of their components, which are often made of high-strength carbon steels with a high carbon equivalent [2]. According to Tomków et al. [3], three methods are used in a water environment: dry welding, local dry cavity welding, and wet welding. Dry welding is the costliest method because it requires constructing and adapting special chambers that isolate the welder and weld metal from the surrounding water [4]. In

addition, depending on the pressure, this method can be carried out at atmospheric pressure or the operating depth [5]. In local dry cavity welding, a special torch adds a gas atmosphere that protects the joint from welding [6]. On the other hand, underwater wet welding is carried out with the arc in direct contact with water. In this sense, Tomków et al. [7] mentioned that the stick electrode has been widely used as a wet welding filler metal; combining low operating and material costs [8–10].

Vashishtha et al. [11] emphasize that the heat generated by the electric arc disassociates the water molecule into hydrogen ions (H<sup>+</sup>) and hydroxide ions (OH<sup>-</sup>). This factor, combined with a high cooling rate, causes the main problems such as

pores and cold cracks. Therefore, researchers in the underwater welding field need to study the operational behavior and the inherent problems therein. One of the research centers specializing in underwater wet welding is Brazil's Robotics, welding, and Simulation Laboratory (LRSS). The LRSS has researched different areas, such as developing consumables and studying operational behavior.

Regarding the development of consumables for underwater wet welding, the LRSS has carried out cutting-edge studies based on the modification of the chemical composition of the filler metals applying the Shielded Metal Arc Welding process: Turani and Bracarense [12] manufactured basic coated electrodes using polytetrafluoroethylene (PTFE) as binder. Santos et al. [13] developed an oxyrutile electrode to decrease hydrogen embrittlement in the welded metal and, consequently, the appearance of cracks that reduce the mechanical strength of welded joints. Using both polarities, Menezes et al. (2019) [14] compared the operational performance of basic electrodes agglomerated with silicate and polymer at a depth of 10 m. The authors concluded that the weld metals obtained with the experimental electrodes agglomerated with polymer presented lower levels of porosity and lower levels of diffusible hydrogen in DCEP than the conventional electrodes. Moreover, this research center has studied the physical phenomena of the electric arc and its relationship with the operational characteristics: Pessoa et al. [15] evaluated the porosity along the weld bead at simulated depths of 50 and 100 m. Moreno-Uribe et al. [16] studied the effect of depth and polarity on penetration and melting rate in an experimental rutile electrode. Moreno-Uribe et al. [17] analyzed the stability of a commercial electrode compared to a consumable developed especially for wet welding.

In addition, high-tech research centers are leading the study of wet welding in Germany and Poland. These institutes have conducted studies on diffusible hydrogen content [18-20] and the evaluation of the weld metal mechanical properties [21–23].

On the other hand, the Flux-Cored Arc Welding (FCAW, 114 according to EN ISO 4063:2023 standard classification of welding processes) process stands as a promising alternative for performing repair and maintenance work in which the welder and joints to be welded are in direct contact with the water environment [24-25]. Jia et al. [26] mention that due to the ease of automation and operation of the FCAW process, productivity can be increased and costs reduced compared to

manual welding. Furthermore, as Moreno-Uribe et al. [27] and Modenesi e Moreno-Uribe [28] stated, the consumable used in the FCAW process allows for adding elements to its flux. Due to this, the literature has demonstrated the importance of studying chemical compositions that will enable obtaining weld metals with unique mechanical [29-31] and metallurgical characteristics [32–34].

In this sense, Ferreira et al. [35] developed tubular wires containing a metallic flux with nickel, chromium, and iron powder, obtaining weld metals with ferritic or austenitic predominance depending on the amount of alpha and gamma-genic elements added in the flux. Li et al. [36] fabricated a 1.6 mm tubular wire using a metal sheet whose chemical composition was 99.5% nickel, containing some minerals needed to protect the arc and the welding pool from the surrounding water, to weld dissimilar joints between low alloy 16Mn and austenitic 304L steel grades. In the next paper by the same research team structural integrity of wet welded joints on two dissimilar materials using two flux-cored wires with different nickel levels in the chemical composition of the flux was described [37]. The advantages of using filler metals containing nickel are related to increasing the Ultimate Tensile Stress (UTS) of the weld metal and its toughness [38], as well as reducing the amount of diffusible hydrogen [39], which allows decreasing the susceptibility of cold cracking [40, 41].

Zhang et al. [42] demonstrated that adding calcium fluoride to the flux-cored wire improves process stability, decreases porosity, and increases the tensile strength of the weld metal. On the other hand, Amaral et al. [43] studied the effect of adding PTFE in rutile-oxidizing flux-cored wires. The authors explained that the high thermal energy resulting from the welding process breaks the polymeric network bonds causing the release of fluor atoms into the arc atmosphere, which form hydrogen fluoride, reducing the diffusible hydrogen content in the weld.

The present work evaluates the electrical behavior of the welding process and characterizes the morphology of the cross sections of weld beads obtained from laboratory-fabricated tubular wires, which were employed to perform wet welding at 0.3 m depth. The importance of this work lies in the fact that it shows the effect of the chemical composition of the wire flux and polarity on weld bead morphology and stability. Moreover, the literature indicates that using flux-cored wires with PTFE additions is promising for reducing the diffusible hydrogen content in the weld metal [43].

## METHODOLOGY

In this study, two tubular wires were developed (as presented in Table 1) with a diameter of 1.6 mm and an average filling rate of 21%. The tubular wires were produced using experimental equipment [44, 45] and were applied onto a 0.5 mm thick and 10 mm wide steel sheet.

Subsequently, weld beads were made in the flat position (PA, 1G) inside a tank with an unsalted water at a depth of 300 mm (shallow depth). The IMC Inversal 300 manufactured by IMC Soldagem was the welding power source, operating at a constant voltage. A mechanized system moved the base metal while the torch was fixed at a 90° angle (see Figure 1). The welding current and arc voltage signals were acquired simultaneously with an SAP V4 system developed by IMC Soldagem, with an acquisition rate of 5 kHz. The welding parameters were obtained from previous research at the LRSS and are shown in Table 2. Moreover, the base metal was a 9.5 mm thick plate of ASTM A-36 steel, the chemical composition of which is shown in Table 3. To evaluate the electrical behavior of the process, 5 s of arc voltage and welding current oscillograms were analyzed, corresponding to a region coinciding with the cuts of the weld bead cross sections,

**Table 2.** Welding parameters

Parameters	Description
Polarity	DCEP (direct current electrode positive) DCEN (direct current electrode negative)
Arc voltage	28 V
Wire feed speed	4.5 m/min
Welding speed	250 mm/min
Stick-out	30 mm
Depth	300 mm

to explore the relationship between the electrical data and the morphology in this specific segment. Furthermore, the average arc voltage and welding current with their respective standard deviation were measured. Moreover, the short circuit index (SCI) was analyzed for a voltage reference value of 14 V, which was selected to divide the process between the stable arc burning region (SAR) and the region of arc voltage values referring to short circuits (SCR). The SCI is explained in Eq. 1 as the ratio between the amount of short circuits and the analysis time defined (5 s).

$$SCI = \frac{\text{Amount of short circuits}}{\text{Time}} \quad (1)$$

The coefficient of variation was used to estimate the stability of the process. The coefficient of

**Table 1.** Chemical composition of tubular wires

Tubular wire type	Rutile + 13% PTFE	Oxidizing + 13% PTFE
Flux composition	40–50% TiO <sub>2</sub> (rutile) 13% PTFE 37–47% gas and slag-generating elements	50–60% Fe <sub>2</sub> O <sub>3</sub> (hematite) 13% PTFE 27–37% gas and slag-generating elements

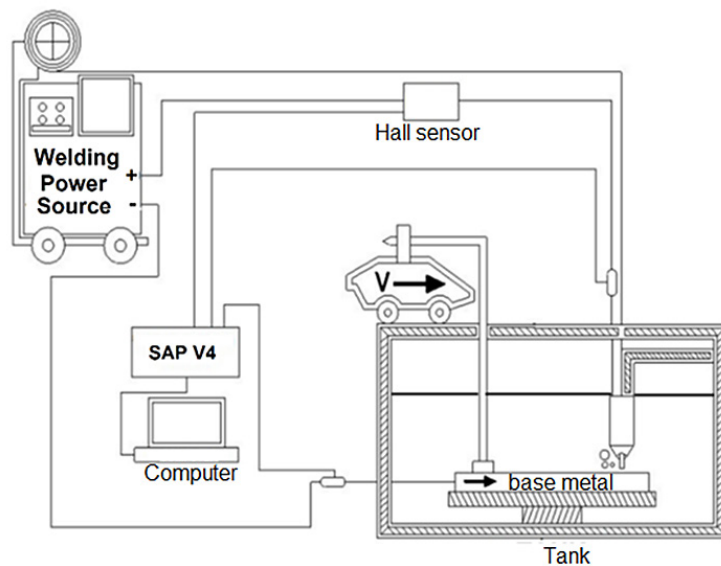


**Figure 1.** Welding process assembly and data acquisition

**Table 3.** Chemical composition of the base metal

C	Mn	Si	P	S	Al	Ni	Cu	Mo	Other elements
0.147	0.6806	0.1935	0.0158	0.009	0.0284	0.0116	0.001	0.003	Balance

variation ( $K_v$ ) was used in assessing the dispersion in relative terms for each condition. In this sense, Castellanos-Gonzalez et al. and Wang et al. [46, 47] suggest that a lower coefficient of variation indicates better stability. In addition, histograms and oscillograms were employed in this study to elucidate the arc behavior during the process. The samples were obtained of weld bead cross-section to determine morphology. The samples were prepared by conventional metallographic techniques, and etched with Nital 5%. Then, photographs were taken using a stereoscopic microscope to characterize the dimensions described in Figure 2. Moreover, weld bead dilution was calculated using Eq. 2.

$$Dilution = \frac{PA}{PA + RA} \times 100 \quad (2)$$

where:  $PA$  – Penetration area,  $RA$  – Reinforcement area

To investigate the effect of the type of flux-cored tubular wire and polarity on the electrical behavior and morphology of the weld bead, three tests were performed for each welding condition. The results were then combined into a matrix for further analysis using one-way ANOVA. The statistical analysis was conducted using Minitab software, with a confidence level of 95%. In this study, one-way ANOVA was used as a statistical tool to determine if there were any significant

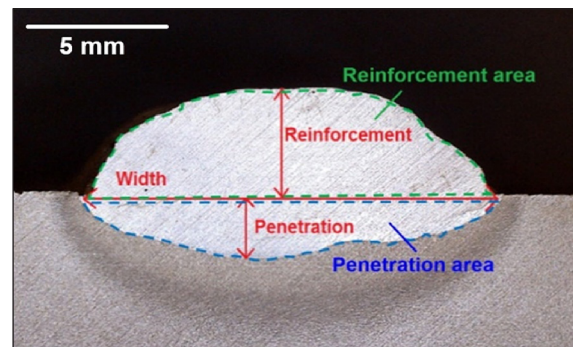


**Figure 2.** Weld bead dimensions

differences in the response variable due to variations in the levels of the selected factors. A significance level of 0.05 was adopted, which means that if the obtained p-value is less than or equal to 0.05, it indicates a meaningful impact of changing the level of the factor on the response variable. On the other hand, a p-value greater than 0.05 suggests a lack of statistical significance [4].

## RESULTS AND DISCUSSION

Table 4 shows the experimental matrix with the values obtained for the arc voltage and welding current for the two experimental tubular wires in both polarities. In addition, the coefficient of

**Table 4.** Electrical parameters for the experimental tubular wires at 0.3 m depth\*

Test	Tubular wire type	Polarity	I (A)	SDI (A)	KvI (%)	U (V)	SDU (V)	KvU (%)	SCI
1	Rutile-base	DCEN	192.9	104.4	54.1	30.7	9.0	29.3	13.4
2	Rutile-base	DCEN	203.4	89.3	43.9	29.8	7.4	24.8	11.4
3	Rutile-base	DCEN	188.3	110.3	58.6	31.0	10.5	33.9	15.0
4	Rutile-base	DCEP	248.1	88.7	35.7	29.0	5.3	18.3	5.2
5	Rutile-base	DCEP	240.7	76.9	31.9	28.8	5.0	17.4	6.6
6	Rutile-base	DCEP	245.6	85.2	34.7	29.3	5.2	17.7	6.0
7	Oxidizing-base	DCEN	241.0	89.0	36.9	30.7	9.0	29.3	13.4
8	Oxidizing-base	DCEN	248.6	86.4	34.8	29.8	7.4	24.8	11.4
9	Oxidizing-base	DCEN	244.8	82.8	33.8	30.2	8.6	28.5	10.9
10	Oxidizing-base	DCEP	239.7	87.2	36.4	29.8	6.6	22.1	2.8
11	Oxidizing-base	DCEP	252.3	89.4	35.4	29.7	5.7	19.2	2.2
12	Oxidizing-base	DCEP	246.0	86.2	35.0	29.5	6.0	20.3	2.5

**Note:** \*Welding current (I), welding current deviation (SDI), coefficient of variation of welding current (KvI), arc voltage (U), arc voltage deviation (SDU), coefficient of variation of arc voltage (KvU), short circuit index (SCI).

variation of arc voltage and welding current and the SCI value were calculated.

The arc voltage and welding current oscillograms are shown in Figure 3 and Figure 4. About metal transfer, it is clear that for both types of tubular wire, there was a predominance of short circuits in both polarities. Nevertheless, the one-way ANOVA verified with a  $p$ -value  $\leq 0.05$  that the effect of polarity on the average SCI value was significant. Therefore, in the DCEP polarity, there was a 67 % decrease in the average SCI value compared to the average value obtained in the DCEN polarity

(Figure 5). This can also be seen in the short circuit region in the histograms of Figure 6 and Figure 7, showing a smaller area in the distribution of arc voltage values for the consumable in the positive connection. Dutra [48] explains that these short circuits are disturbances in the process due to arc extinction at a specific frequency when the arc voltage value is below the voltage reference value of 5 V. Guo et al. [49] classified this behavior within a short-circuit transfer mode. The authors evaluated the detachment frequency and size of the molten droplets using the X-ray technique. However, Guo

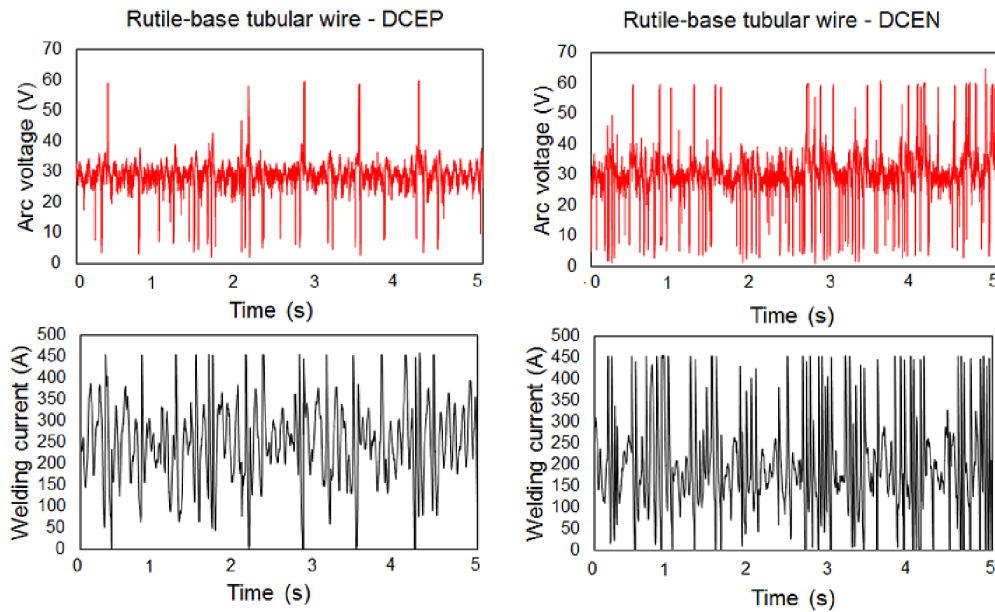


Figure 3. Arc voltage and welding current oscillograms for the rutile-base tubular wire: DCEP and DCEN

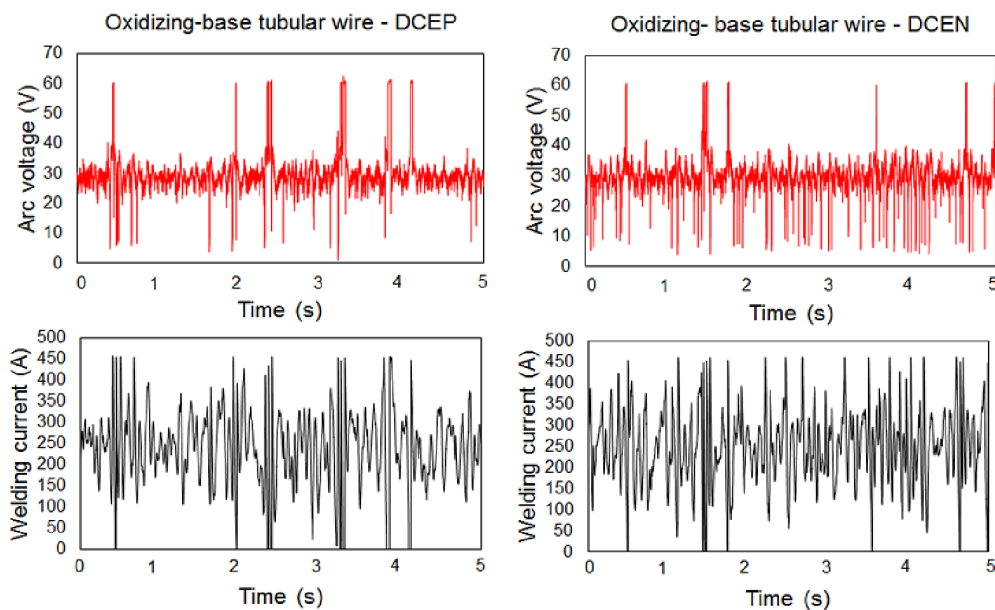
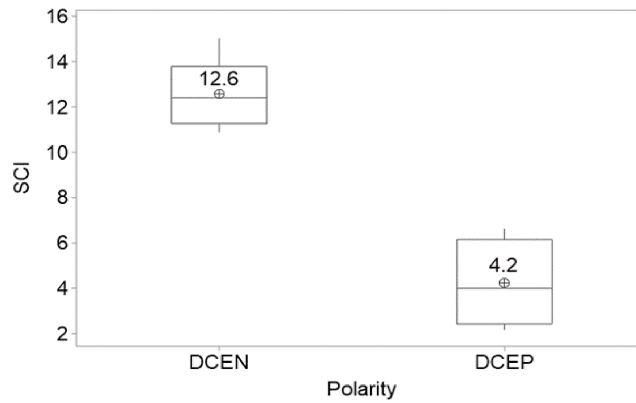
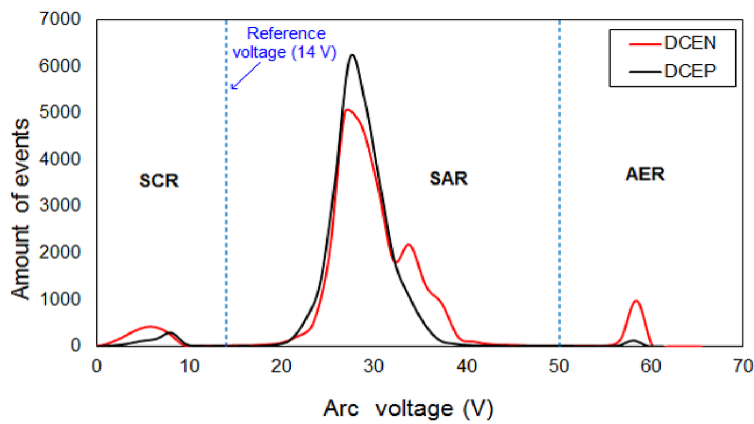


Figure 4. Arc voltage and welding current oscillograms for the oxidizing-base tubular wire: DCEP and DCEN



**Figure 5.** Effect of polarity on the average SCI value. The boxplots were corroborated using one-way ANOVA with a 95% confidence level



**Figure 6.** Histogram for the rutile-base tubular wire: DCEP and DCEN: SCR – short circuit region, SAR – stable arc burning region, AER – arc extinction region

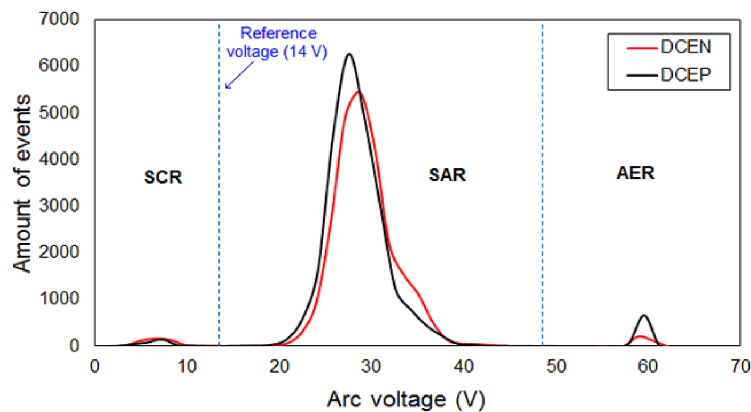


**Figure 7.** Histogram for the oxidizing-base tubular wire: DCEP and DCEN: SCR –short circuit region, SAR – stable arc burning region, AER – arc extinction region

et al. [49] mention that this type of transfer can be divided depending on the forces involved and the welding current and arc voltage levels present in surface tension transfer and explosive short circuit transfer. The arc voltage and welding current oscillograms show that when the arc voltage drops

below 14 V, the welding current exceeds 450 A. At this point, a short circuit is established, and the liquid metal is transferred to the weld pool due to the combination of the magnitudes of the electromagnetic force and the surface tension [49]. After this event, the source dynamics allowed the restoration

of the arc voltage value to the one configured in the process (28 V). On the other hand, Castellanos-Gonzalez et al. [46] commented that when the arc voltage reaches the value of 60 V (commonly the power source open circuit voltage), the welding current value decreases close to 0 A, causing the arc shutdown (arc extinction region in the histograms).

The average welding current value for the oxidizing-base tubular wire showed no significant change in the two polarities (values from Table 4). In contrast, for the rutile-base tubular wire, a 26 % increase in the average value of the welding current was observed in reverse polarity (values from Table 4). This phenomenon might be related to voltage drops in the arc-electrode connection, as Solano et al. [50] described. In the case of oxidizing-base tubular wire, there was probably no difference in the sum of the anode and cathode fall values ( $U_a+c$ ). Instead, for the rutile-base tubular wire, there was a lower average

welding current for direct polarity, which generated considerable energy. Therefore, less welding current is needed to melt the experimental tubular wire in this polarity configuration when the source operates at a constant voltage.

Figure 8 shows a high positive correlation between the coefficient of variation of arc voltage (KvU) and the coefficient of variation of welding current (KvI). The method used to measure the relationship between these variables was Pearson's Correlation [51]. Hence, only KvU was used to estimate the stability of the process to avoid redundancy in explaining the phenomenon. In this sense, it can be seen that the effect of polarity on the stability of the process is significant. The one-way ANOVA with a p-value  $\leq 0.05$  verified that the average value of the arc voltage coefficient of variation decreased by 32 % with the DCEP polarity compared to the DCEN polarity (Figure 9). In addition, the histograms' stable arc burning region

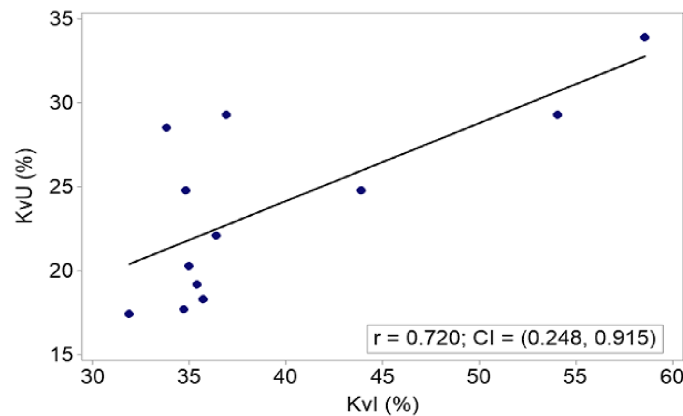


**Figure 8.** Scatter plot showing correlation between KvI and KvU.  $r$  is Pearson's correlation coefficient and  $CI$  is the confidence interval

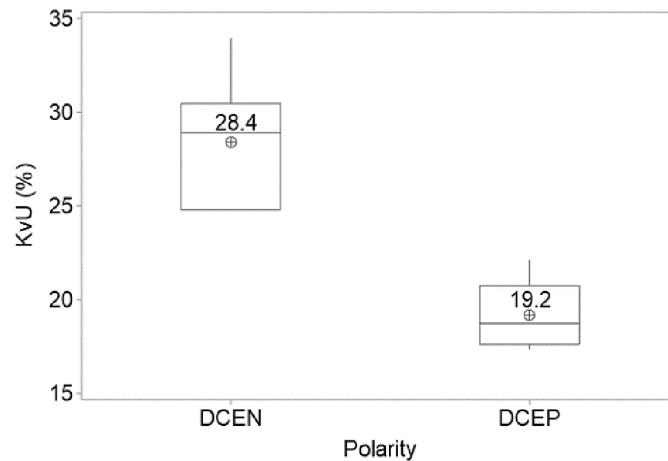


**Figure 9.** Effect of polarity on the average KvU value. The boxplots were corroborated using one-way ANOVA with a 95% confidence level

(SAR) also shows higher stability in reverse polarity. As explained by Bauné et al. [52], it is possible to characterize a trustworthy electric arc by analyzing the height and width of the histograms. Thus, in the DCEP polarity, it can be seen that there was a more stable process because the SAR of the histograms showed a high and narrow peak.

Furthermore, there was no statistical significance after executing the one-way ANOVA of the effect of the type of electrode-wire on the coefficient of variation of the arc voltage ( $p$ -value > 0.05). Therefore, this work has demonstrated that experimental tubular wires with an oxidizing-base can be obtained with comparable stability to those with a rutile-base.

Table 5 presents the morphology characteristics of the weld beads obtained with the two experimental tubular wires in DCEP and DCEN polarities. It can be observed that for the oxidizing-base

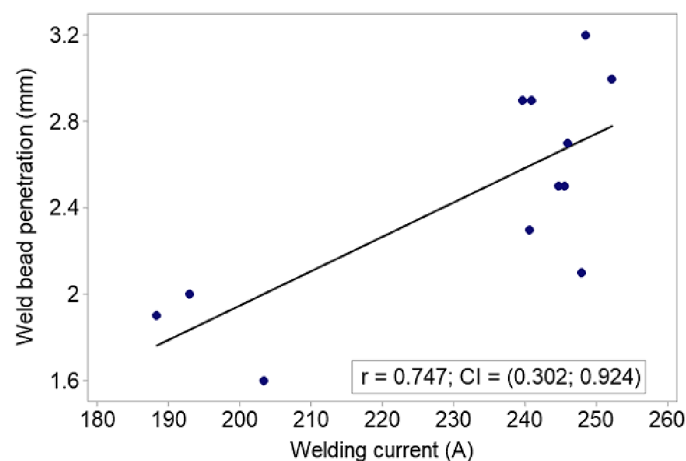
tubular wire, there was no notable difference in the penetration value when comparing the two polarities. On the contrary, for the DCEN polarity configuration with the rutile-base tubular wire, the average penetration value of the weld bead was 20 % lower than the reverse polarity.

Figure 10 shows the positive correlation between welding current and weld bead penetration. Pearson’s correlation coefficient ( $r = 0.747$ ) indicates a high correlation between the variables compared. Karadeniz et al. [53] described that the influence of welding current on penetration is approximately 2.5 times greater than arc voltage and welding speed. Moreover, Assunção and Bracarense [54] explain that a higher energy density due to the welding current increases the penetration of the weld bead.

Figure 11 shows the boxplot relating the type of experimental tubular wire to the penetration

**Table 5.** Weld bead morphology of experimental tubular wires in 0.3 depth

Test	Tubular wire type	Polarity	Penetration (mm)	Width (mm)	Reinforcement (mm)	Dilution (%)
1	Rutile-base	DCEN	2.0	8.0	4.6	32.5
2	Rutile-base	DCEN	1.6	8.5	4.5	35.0
3	Rutile-base	DCEN	1.9	8.4	4.7	31.0
4	Rutile-base	DCEP	2.1	9.0	3.1	48.9
5	Rutile-base	DCEP	2.3	9.5	3.2	48.1
6	Rutile-base	DCEP	2.5	9.3	3.0	47.0
7	Oxidizing-base	DCEN	2.9	9.8	3.0	51.0
8	Oxidizing-base	DCEN	3.2	9.6	3.2	54.2
9	Oxidizing-base	DCEN	2.5	9.4	3.3	52.1
10	Oxidizing-base	DCEP	2.9	10.6	2.8	51.4
11	Oxidizing-base	DCEP	3.0	10.3	2.4	55.7
12	Oxidizing-base	DCEP	2.7	10.0	2.5	53.5



**Figure 10.** Scatter plot showing correlation between Welding current and weld bead penetration:  $r$  is Pearson’s correlation coefficient and  $CI$  is the confidence interval

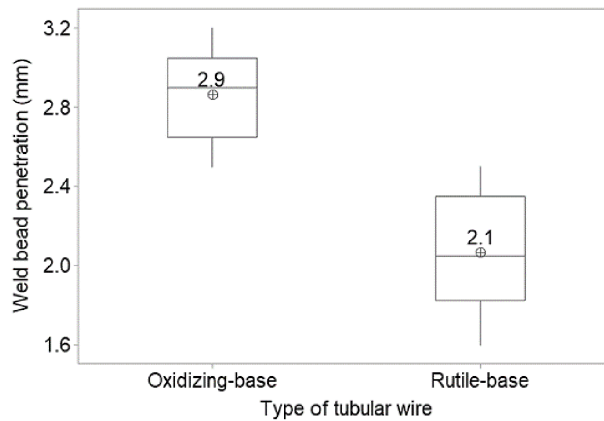


**Figure 11.** Effect of tubular wire type on the average weld bead penetration value. The boxplots were corroborated using one-way ANOVA with a 95% confidence level

value. The one-way ANOVA verified that the effect of tubular wire type was significant on the average penetration value ( $p\text{-value} \leq 0.05$ ). In this sense, the average penetration value was 38 % higher for the oxidizing-based tubular wire than for the rutile-based tubular wire. The presence of  $\text{Fe}_2\text{O}_3$  in the oxidizing-base tubular wire likely contributes to these higher penetrations due to increased oxygen levels. Amaral et al. [43] observed elevated oxygen in rutile-oxidizing tubular wires. In line with this, Heiple and Burgardt [55] found in Gas Metal Arc Welding (GMAW) experiments that higher oxygen in the shielding gas results in a weld metal with deeper penetration.

Figure 12 shows the cross-sections of the weld beads obtained with the two experimental tubular wires in the two polarities. It can be seen that the weld bead reinforcement is higher in the

weld beads obtained with the rutile-based tubular wire, and the difference in weld bead reinforcement in the DCEN polarity is more noticeable. In addition, the boxplot in Figure 13 shows that the average value of the weld bead reinforcement is 35 % higher in the rutile-based tubular wire, with a  $p\text{-value} \leq 0.05$ .

Figure 14 shows that the average value of the weld bead width is 13.7% greater in the oxidizing-base tubular wire compared to the rutile-base tubular wire, with a  $p\text{-value} \leq 0.05$ . Moreover, Figure 15 shows that the average value of weld bead dilution is 31.2 % higher in the oxidizing-base tubular wire than in the rutile-base tubular wire, with a  $p\text{-value} \leq 0.05$ . This difference is why the highest average penetration and width values were obtained with the oxidizing-base tubular wire, which increases the penetration area and, consequently, the dilution

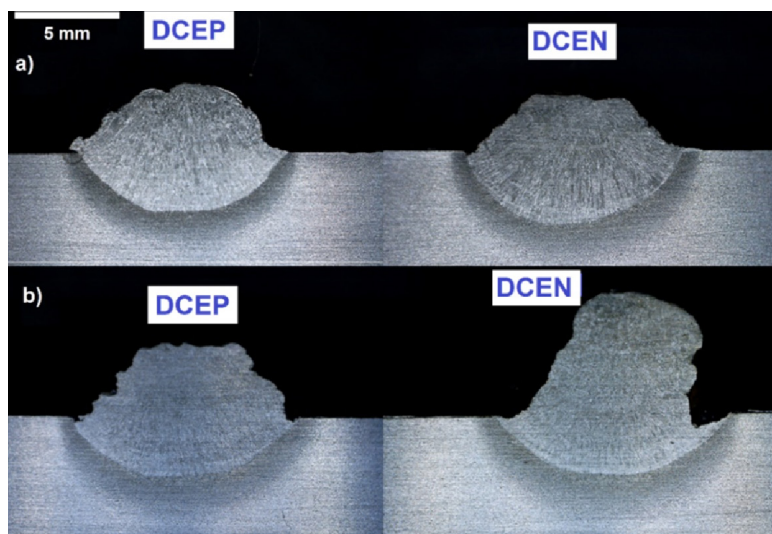


**Figure 12.** Cross sections of weld beads (a) oxidizing-base tubular wire (b) rutile-base tubular wire

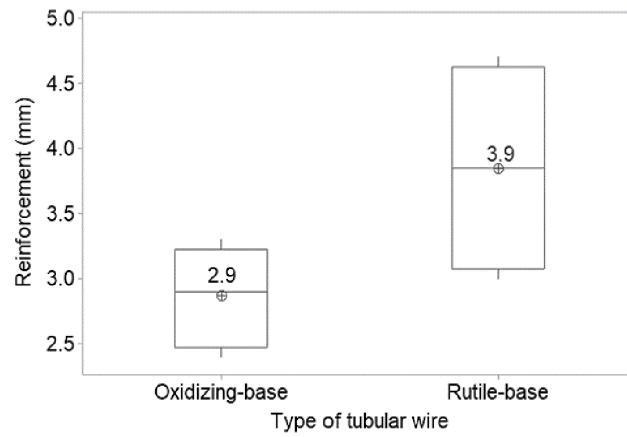


**Figure 13.** Effect of tubular wire type on the average weld bead reinforcement value. The boxplots were corroborated using one-way ANOVA with a 95% confidence level

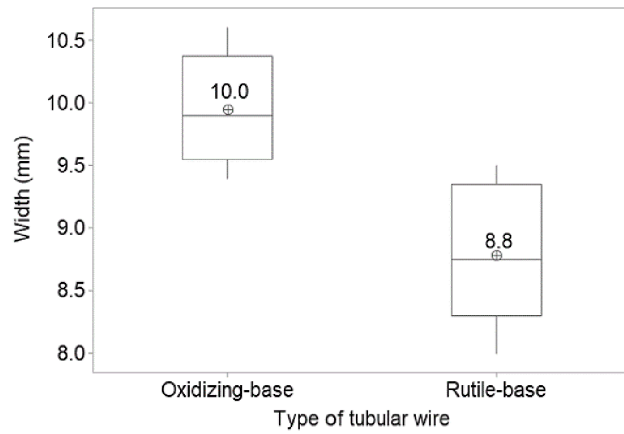


**Figure 14.** Effect of tubular wire type on the average weld bead width value. The boxplots were corroborated using one-way ANOVA with a 95% confidence level

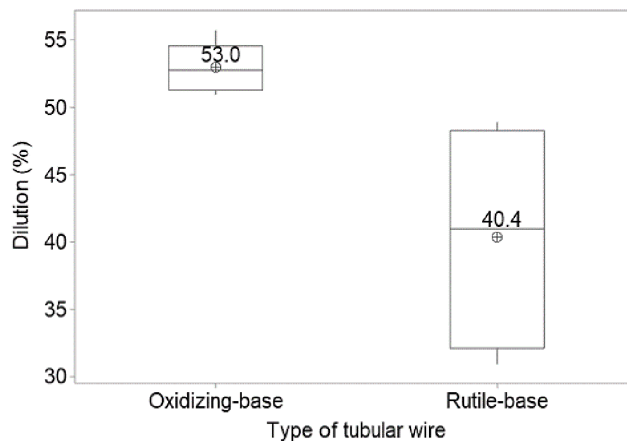


**Figure 15** Effect of tubular wire type on the average weld bead dilution value. The boxplots were corroborated using one-way ANOVA with a 95% confidence level

of the weld bead. Figure 16 displays 50 mm sections of mid-section of the weld beads obtained. The beads presented porosity at the top, undercuts,

and excessive reinforcement. These discontinuities are common in wet welds [56]. Furthermore, the oxidizing-base tubular wire deposited weld

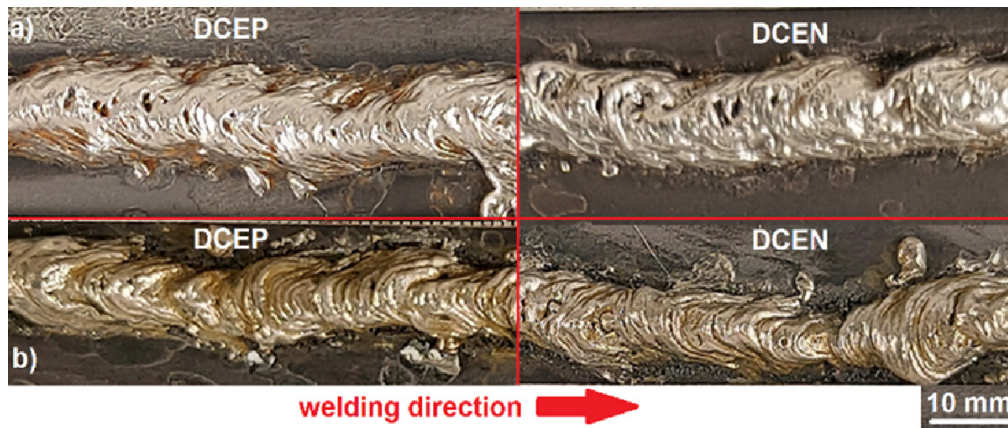


Figure 16. Top view of the weld beads (a) oxidizing-base tubular wire (b) rutile-base tubular wire

beads with greater surface porosity in both polarities than those obtained with the rutile-base tubular wire. On the other hand, higher number of undercuts were observed in the weld beads deposited with the rutile-base tubular wire in both polarities. Moreover, excessive reinforcement was noted for the weld bead obtained with the rutile-base tubular wire in direct polarity (consistent with Figure 12) and a fusion incomplete in some areas. According to Chen et al. [57], the incomplete fusion in the weld bead is attributed to arc extinction.

As can be seen, the weld bead produced using the oxidizing-base experimental tubular wire in reverse polarity demonstrates notable advantages, exhibiting minimal undercuts and a complete absence of pores in the cross-section. Any pores present are mainly located at the top of the weld bead reinforcement. The lack of cracks, excellent wettability, and acceptable quality positions this experimental tubular wire as an up-and-coming alternative. Furthermore, the presence of reinforcement pores is practically inconsequential in industrial applications, as it is common practice for welders to remove such reinforcements during repair work through grinding [58, 59]. Importantly, this experimental tubular wire showcases operability and maintenance of the arc that is acceptable and comparable to those achieved with rutile-base experimental tubular wire. It is crucial to highlight that oxidizing electrodes effectively diminish the diffusible hydrogen content in the weld metal, thereby mitigating susceptibility to hydrogen cracking [60–62]. Consequently, the anticipated low diffusible hydrogen content in the weld metal deposited with the oxidizing-base tubular wires further underscores their potential as a superior choice in welding applications [63, 64].

## CONCLUSIONS

The present work demonstrated the study of arc stability, short circuit dynamics and the characterization of the morphology of weld beads produced with two experimental tubular wires. In general, both tubular wires showed acceptable weldability and weld bead appearance with acceptable quality. The main findings are summarized as follows:

- The experimental oxidizing-base tubular wire on DCEP polarity emerged as a promising alternative due to its exceptional arc stability and satisfactory weld bead quality. This study underscores the significance of considering tubular wire type and polarity in welding processes, as operational behavior and weld bead quality vary accordingly.
- DCEN polarity adversely affected the arc stability of the rutile-base tubular wire, leading to increased discontinuities; however, adjusting parameters like arc voltage and welding speed can enhance process performance and weld bead quality.
- Both polarities exhibited a prevalence of short circuits, but DCEP polarity demonstrated a significant 66.7% reduction in the average Short Circuit Index (SCI) compared to DCEN polarity for both tubular wires.
- The oxidizing-base tubular wire consistently achieved higher average weld bead penetration than the rutile-base tubular wire in both polarities, with DCEN polarity for the rutile-base tubular wire showing lower penetration associated with welding current.
- The average value of the weld bead reinforcement is higher in the rutile-based tubular wire compared to the oxidizing-based tubular wire.

- The average value of the weld bead width was greater in the oxidizing-base tubular wire compared to the rutile-base tubular wire.
- The average value of weld bead dilution is higher in the oxidizing-base tubular wire than in the rutile-base tubular wire. This difference is why the highest average penetration and width values were obtained with the oxidizing-base tubular wire, which increases the penetration area and, consequently, the dilution of the weld bead.

## Acknowledgments

The authors would like to thank the Robotics, Welding and Simulation Laboratory – LRSS (Federal University of Minas Gerais) for its support in the development of this work. This study was financed in part by the Coordenação de Aperfeiçoamento de Pessoal de Nível Superior – Brazil (CAPES) – Finance Code 001.

## REFERENCES

1. Rogalski G, Fydrych D, Łabanowski J. Underwater wet repair welding of API 5L X65M pipeline steel. *Polish Maritime Research* 2017; 24(s1): 188–194. <https://doi.org/10.1515/pomr-2017-0038>.
2. Ortiz, J.L., Moreno-Uribe, A.M., Acevedo, B.R., Lima, E.J., Arias, A.R. 2021 Application of computer vision techniques for contour detection in underwater wet welding: an exploratory study. *Journal of Physics: Conference Series*, 2046(1), 012072. IOP Publishing. <https://doi.org/10.1088/1742-6596/2046/1/012072>
3. Tomków J., Świerczyńska A., Landowski M., Wolski A., Rogalski G. Bead-on-plate underwater wet welding on S700MC steel. *Advances in Science and Technology Research Journal*, 2021; 15: 288–296. <https://doi.org/10.12913/22998624/140223>.
4. Tomków, J. Weldability of Underwater Wet-Welded HSLA Steel: Effects of Electrode Hydrophobic Coatings. *Materials* 2021; 14: 1364. <https://doi.org/10.3390/ma14061364>.
5. Han K., Cao Y., Li H., Hu C., Wang Z., Liu D., Wang J., Zhu Q. Influence of Butter Layer Thickness on Microstructure and Mechanical Properties of Underwater Wet 16Mn/304L Dissimilar Welded Joint. *Materials* 2023; 16. <http://dx.doi.org/10.3390/ma16206646>.
6. Rogalski G., Świerczyńska A., Fydrych D. Determination of t8/5 cooling times for underwater local dry welding of steel. *Marine Structures* 2023; 91. <https://doi.org/10.1016/j.marstruc.2023.103477>.
7. Tomków J., Fydrych D., Łabanowski, J. Effect of water salinity on properties of multipass underwater wet manual metal arc welded joints. *Welding in the World* 2023; 67: 2381–2390. <https://doi.org/10.1007/s40194-023-01554-y>.
8. Santos V., Bracarense A.Q., Pessoa E., Marinho R., Rizzo F., Nóbrega A., Junior R., Monteiro M., Rebello J Prediction of hydrogen cracking in the wet welding of structural steels with ferritic stick electrodes down to 20 m. *Journal of Materials Research and Technology* 2021; 15: 5787–5802. <https://doi.org/10.1016/j.jmrt.2021.11.003>.
9. Pessoa E., Liu S. The State of the Art of Underwater Wet Welding Practice: Part 1. *Welding Journal* 2021; 100: 1–10. <https://doi.org/10.29391/2021.100.011>.
10. Pessoa E., Liu S. The State of the Art of Underwater Wet Welding Practice: Part 2. *Welding Journal* 2021; 100: 171–182. <https://doi.org/10.29391/2021.100.014>.
11. Vashishtha P., Watta R., Pandey S., Bhadauria N. Problems encountered in underwater welding and remedies – a review. *Materials Today* 2022; 64:1433–1439. <https://doi.org/10.1016/j.matpr.2022.04.634>.
12. Turani C., Bracarense A.Q. The influence of PTFE used as basic covered electrode binder on weld metal acicular ferrite formation. *Welding International* 2016; 30: 359–371. <https://doi.org/10.1080/09507116.2015.1096507>.
13. Santos V., Bracarense A.Q., Pessoa E., Marinho R., Rizzo F., Junior R., Monteiro M Development of oxyrutile low alloy ferritic electrode for wet welding. *Journal of Materials Research and Technology* 2012, 21: 1223–1247. <https://doi.org/10.1016/j.jmrt.2022.09.088>
14. Menezes, P.H.R., Pessoa, E.C.P., Bracarense, A.Q. Comparison of underwater wet welding performed with silicate and polymer agglomerated electrodes. *Journal of Materials Processing Technology* 2019, 266, 63–72.
15. Pessoa E., Bracarense A., Maluf E., Liu S., Perez-Guerrero F. Porosity variation along multipass underwater wet welds and its influence on mechanical properties. *Journal of Materials Processing Technology* 2006; 179: 239–243. <https://doi.org/10.1016/j.jmatprotec.2006.03.071>.
16. Moreno-Uribe A., Bracarense A., Pessoa E. The Effect of Polarity and Hydrostatic Pressure on Operational Characteristics of Rutile Electrode in Underwater Welding. *Materials* 2020; 13: 5001. <https://doi.org/10.3390/ma13215001>.
17. Moreno-Uribe A., Bracarense A., Pessoa E., Santos V. Influência da Polaridade Sobre a Estabilidade do Processo de Soldagem Subaquática Molhada com Eletrodo Revestido. *Soldagem & Inspeção* 2017, 22: 429–441. <https://doi.org/10.1590/0104-9224/>

- SI2204.13. (in Spanish)
18. Bratz O., Klett J., Wolf T., Henkel K., Maier H., Hassel T. Induction Heating in Underwater Wet Welding-Thermal Input, Microstructure and Diffusible Hydrogen Content. *Materials* 2022; 15. <https://doi.org/10.3390/ma15041417>.
  19. Klett, J., Hassel, T. Influence of stick electrode coating's moisture content on the diffusible hydrogen in underwater wet shielded metal arc welding. *Advances in Materials Science* 2020; 20(4): 27–37. <https://doi.org/10.2478/adms-2020-0020>.
  20. Klett J., Oliver G., Schmidt E., Linowitzki V. Effect of the water depth on the hydrogen content in SMAW wet welded joints. *SN Applied Sciences* 2020; 2: 1–14. <https://doi.org/10.1007/s42452-020-3066-8>.
  21. Younes R., Tomków J., Idir A., Boudjit S., Bradai M.A. Mechanical and structural behavior of high-strength low-alloy steel pad welded by underwater wet welding conditions. *The International Journal of Advanced Manufacturing Technology* 2023; 129(11), 5615–5624.
  22. Tomków J., Landowski M., Fydrych D., Rogalski G. Underwater wet welding of S1300 ultra-high strength steel. *Marine Structures* 2022; 81. <https://doi.org/10.1016/j.marstruc.2021.103120>.
  23. Fydrych D., Raczko P., Świerczyńska A., Landowski M., Wolski A., Rogalski G. Effect of Arc Strikes on High Strength Low Alloy Steels Welded by SMAW. *Advances in Science and Technology Research Journal* 2023; 17: 160–169. <https://doi.org/10.12913/22998624/166061>.
  24. Chen H., Guo N., Shi X., Du Y., Feng J., Wang G. Effect of water flow on the arc stability and metal transfer in underwater flux-cored wet welding. *Journal of Manufacturing Processes* 2018; 31: 103–115. <https://doi.org/10.1016/j.jmapro.2017.11.010>.
  25. Castellanos-Gonzalez M., Moreno-Urbe A., Rodríguez A., Jácome J. Particularidades de la transferencia metálica y la aplicación de corriente pulsada en soldadura submarina. *Revista UIS Ingenierías* 2022; 21: 1–14. <https://doi.org/10.18273/revuin.v21n4-2022001>. (in Spanish)
  26. Jia C., Wu J., Han Y., Zhang Y., Yang Q., Wu C. Underwater Pulse-Current FCAW — Part 1: Waveform and Process Features. *Welding Research* 2020; 99: 135–145 <https://doi.org/10.29391/2020.99.013>.
  27. Moreno-Urbe, A.M., Vaccari, L., Bracarense, A.Q., Maier, H.J., Hassel, T. Operational performance and metal droplet formation in pulsed-shielded metal arc underwater welding. *Archives of Civil and Mechanical Engineering* 2024; 24(2), 94.
  28. Modenesi P.J., Moreno-Urbe A.M. Introduction to the physics of the electric arc and its application to the welding of metals. *Ecoe Ediciones*, 2022 Bogotá.
  29. Rodriguez A., Bracarense A. Velocidade de Propagação de Trinca por Fadiga de Soldas Subaquáticas Molhadas: Avaliação Fora da Água. *Soldagem & Inspeção* 2015; 20: 403–411. <https://doi.org/10.1590/0104-9224/SI2004.07>. (in Portuguese)
  30. Świerczyńska A., Varbai B., Pandey C., Fydrych D. Exploring the trends in flux-cored arc welding: scientific analysis approach. *The International Journal of Advanced Manufacturing Technology* 2023; 1–24. <https://doi.org/10.1007/s00170-023-12682-6>.
  31. Soares L., Modenesi P., Barbosa L., Rodriguez A. Fatigue crack growth rates on the weld metal of high heat input submerged arc welding. *International Journal of Fatigue* 2019; 119: 43–51. <https://doi.org/10.1016/j.ijfatigue.2018.09.020>.
  32. Costa P., Altamirano G., Ochoa R., Reséndiz E., Guía L., Ramirez L. Optimization of welding parameters in underwater wet FCAW on a structural steel using support vector regression and sequential quadratic programming. *The International Journal of Advanced Manufacturing Technology* 2022, 121: 4225–4236. <https://doi.org/10.1007/s00170-022-09584-4>.
  33. Parshin S., Levchenko A., Maystro A. Metallurgical Model of Diffusible Hydrogen and Non-Metallic Slag Inclusions in Underwater Wet Welding of High-Strength Steel. *Metals* 2020; 10: 1498. <https://doi.org/10.3390/met10111498>.
  34. Trembach B., Silchenko Y., Balenko O., Hlachev D., Kulahin K., Heiko H., Trembach, I. Study of the hardfacing process using self-shielding flux-cored wire with an exothermic addition with a combined oxidizer of the Al-(CuO/Fe<sub>2</sub>O<sub>3</sub>) system. *The International Journal of Advanced Manufacturing Technology* 2024; 134: 309–335. <https://doi.org/10.1007/s00170-024-14115-4>.
  35. Ferreira M., Liberato F., Bracarense A. Desenvolvimento de arame tubular com fita de aço carbono AISI 1006 e fluxo metálico contendo níquel, cromo e ferro em pó para a soldagem FCAW: development of a tubular wire with AISI 1006 carbon steel strip and metallic flux containing nickel, chromium and iron powder for FCAW. *74o Congresso Anual da ABM* 2019; 74: 886–894. <https://doi.org/10.5151/2594-532733302>. (in Portuguese)
  36. Li H., Liu D., Yan Y.T., Guo N., Feng J.C. Microstructural characteristics and mechanical properties of underwater wet flux-cored wire welded 316L stainless steel joints. *Journal of Materials Processing Technology* 2016, 238: 423–430. <https://doi.org/10.1016/j.jmatprotec.2016.08.001>.
  37. Wei P., Li H., Liu J., Li S., Zha Y., Zhu Q., Lei Y. The effect of water environment on microstructural characteristics, compositional heterogeneity and microhardness distribution of 16Mn/304L dissimilar welded joints. *Journal of Manufacturing Processes* 2020; 56, 417–427. <https://doi.org/10.1016/j.jmapro.2020.05.006>.

38. Guo N., Guo W., Du Y., Fu Y., Feng J. Effect of boric acid on metal transfer mode of underwater flux-cored wire wet welding. *Journal of Materials Processing Technology* 2015; 223: 124–128. <https://doi.org/10.1016/j.jmatprotec.2015.04.002>.
39. Li H., Duo L., Song Y., Yan Y., Guo N., Feng J. Microstructure and mechanical properties of underwater wet welded high-carbon-equivalent steel Q460 using austenitic consumables. *Journal of Materials Processing Technology* 2017; 249: 149–157. <https://doi.org/10.1016/j.jmatprotec.2017.06.009>.
40. Klett J, Mattos I, Maier H, Silva R, Hassel T. Control of the diffusible hydrogen content in different steel phases through the targeted use of different welding consumables in underwater wet welding. *Materials and Corrosion* 2021; 72: 504–516. <https://doi.org/10.1002/maco.202011963>.
41. Ma Q., Li H., Liu S., Liu D., Wang P., Zhu Q., Lei Y. Comparative Evaluation of Self-Shielded Flux-Cored Wires Designed for High Strength Low Alloy Steel in Underwater Wet Welding: Arc Stability, Slag Characteristics, and Joints' Quality. *Journal of Materials Engineering and Performance* 2022; 31: 5244–5244. <https://doi.org/10.1007/s11665-022-06683-x>.
42. Zhang X., Guo N., Xu C., Du Y., Chen B., Feng J. Influence of  $\text{CaF}_2$  on microstructural characteristics and mechanical properties of 304 stainless steel underwater wet welding using flux-cored wire. *Journal of Manufacturing Processes* 2019; 45: 138–146. <https://doi.org/10.1016/j.jmapro.2019.07.003>.
43. Amaral E., Moreno-Uribe A., Bracarense A. Effects of PTFE on operational characteristics and diffusible H and O contents of weld metal in underwater wet welding. *Journal of Manufacturing Processes* 2021; 61: 270–279. <https://doi.org/10.1016/j.jmapro.2020.11.018>.
44. Fagundes J, Moreno-Uribe A, Ribeiro P, Arias R, Bracarense A. Formation of TiC by the application of Ti6Al4V machining chips as flux compounds of tubular wires. *Journal of Physics* 2018; Conference Series 1126. <https://doi.org/10.1088/1742-6596/1126/1/012027>.
45. Castellanos-Gonzalez M., Moreno-Uribe A., Prada G., Jácome L., Rodríguez A. Manufactura De Alambre Tubular Autoprotegido Y Evaluación De Condiciones Operacionales En Soldadura Submarina. *Investigación e Innovación en Ingenierías* 2021; 9: 167–179. <https://doi.org/10.17081/invinno.9.1.4015>. (in Spanish)
46. Castellanos-Gonzalez O., Moreno-Uribe A., Ramón S., Jácome J. Evaluación de la transferencia metálica y estabilidad del proceso GMAW. *Revista UIS Ingenierías* 2020; 20: 47–60. <https://doi.org/10.18273/revuin.v20n3-2021003>. (in Spanish)
47. Wang J., Sun Q., Zhang T., Tao X., Jin P., Feng J. 2019. Arc stability indexes evaluation of ultrasonic wave-assisted underwater FCAW using electrical signal analysis. *The International Journal of Advanced Manufacturing Technology* 103: 2593–2608. <https://doi.org/10.1007/s00170-019-03463-1>.
48. Dutra J. MIG/MAG - transferência metálica por curto-circuito—Fontes de soldagem versus gases do arco. *Soldagem & Inspeção* 2008; 13: 19–24. (in Portuguese)
49. Guo N., Fu Y., Feng J., Du Y., Deng Z., Wang M., Tang D. Classification of metal transfer mode in underwater wet welding. *Welding Journal* 2016; 95: 133–140.
50. Solano, J.L.O., Moreno-Uribe., A.M., Jaimes, B.R.A., Okuyama, M.P., Arias, A.R., Silva, R.H. G.E. Detection and characterization of metal transfer in GMAW using computational vision algorithms. *The International Journal of Advanced Manufacturing Technology* 2023, 128(7–8), 3415–3425.
51. Kluz R., Bucior M., Kubit A., Trzepieciński T., Antosz K., Faes K. Analytical Approach for Forecasting the Load Capacity of the EN AW-7075-T6 Aluminum Alloy Joints Created Using RFSSW Technology. *Materials* 2024; 17(7): 1529. <https://doi.org/10.3390/ma17071529>.
52. Bauné E., Bonnet C., Liu S. Assessing metal transfer stability and spatter severity in flux cored arc welding. *Science and Technology of Welding and Joining* 2011, 6: 139–148. <http://dx.doi.org/10.1179/136217101101538677>.
53. Karadeniz E., Ozsarac U., Yildiz C. The effect of process parameters on penetration in gas metal arc welding processes. *Materials & Design* 2007 28: 649–656. <https://doi.org/10.1016/j.matdes.2005.07.014>.
54. Assunção M., Bracarense A A novel strategy to improve melting efficiency and arc stability in underwater FCAW via contact tip air chamber. *Journal of Manufacturing Processes* 2023, 104: 1–16. <https://doi.org/10.1016/j.jmapro.2023.08.054>.
55. Heiple C., Burgardt P. Effects of  $\text{SO}_2$  shielding gas additions on GTA weld shape. *AWS 66TH Annual Convention Welding Research Supplement*. 1985, 159–162.
56. Mazzaferro J., Machado I. Study of arc stability in underwater shielded metal arc welding at shallow depths. *Proceedings of the Institution of Mechanical Engineers, Part C: Journal of Mechanical Engineering Science* 2009, 223: 699–709. <https://doi.org/10.1243/09544062JMES1>.
57. Chen J, Wen Z, Jia C, Zhao B, Wu C. The mechanisms of underwater wet flux-cored arc welding assisted by ultrasonic frequency pulse high-current. *Journal of Materials Processing Technology* 2022, 304. <https://doi.org/10.1016/j.jmatprotec.2022.117567>.
58. Rodriguez-Sanchez J.E, Rodriguez-Castellanos A., Perez-Guerrero F., Carbajal-Romero M.F., Liu S. Offshore fatigue crack repair by grinding and

- wet welding. *Fatigue & Fracture of Engineering Materials & Structures* 2010, 34: 487–497. doi: 10.1111/j.1460-2695.2010.01541.x.
59. Mendes G., Bracarense A.Q., Pessoa E.C.P., Nazare C. Efeito da técnica de esmerilhamento do cordão na dureza da ZTA de soldas multipasses subaquáticas molhadas. *Soldagem & Inspeção*. 2020, 25: 25–38. <https://doi.org/10.1590/0104-9224/SI25.38>. (in Portuguese)
60. Medeiros R.C. 1997 Effect of oxidizing electrodes and polarity on hydrogen mitigation in underwater wet welding. Colorado School of Mines. Arthur Lakes Library.
61. Pope A.M., Teixeira J.C.G., Dos Santos V.R., Paes M.T.P., Liu S. The Effect of Nickel on the Mechanical Properties of High-Oxygen Underwater Wet Welds. *J. Offshore Mech. Arct. Eng.*, 1996. 118: 165–168. <https://doi.org/10.1115/1.2828827>
62. Pope A.M. Oxygen and hydrogen control in shielded metal underwater wet welding. Colorado School of Mines 1995, Arthur Lakes Library.
63. Amaral, E.C., Jácome-Carrascal, J.L., Moreno-Uribe, A.M., Bracarense, A.Q. Influence of the formulation of a flux-cored wire on the microstructure and hardness of welded metal. In *Journal of Physics: Conference Series* (Vol. 2118, No. 1, p. 012010). 2021. IOP Publishing. <https://doi.org/10.1088/1742-6596/2118/1/012010>
64. Uribe, A.M.M., Bracarense, A.Q., Pessoa, E.C., de Almeida Carvalho, G.M., da Silva, N.N. Metodología de Diseño de una Escotilla de Inspección para Recipientes a Presión. *Investigación e Innovación en Ingenierías* 2017; 5(1), 8–23. <https://doi.org/10.17081/invinno.5.1.2613> (in Spanish)